Research article

Free convection of a suspension containing nano-encapsulated phase change material in a porous cavity; local thermal non-equilibrium model

Mohammad Ghalambaz [a,b,*], Seyed Mohsen Hashem Zadeh [c], S.A.M. Mehryan [d], Amir Haghparast [c], Hossein Zargartalebi [e]

[a] Metamaterials for Mechanical, Biomechanical and Multiphysical Applications Research Group, Ton Duc Thang University, Ho Chi Minh City, Viet Nam
[b] Faculty of Applied Sciences, Ton Duc Thang University, Ho Chi Minh City, Viet Nam
[c] Department of Mechanical Engineering, Shahid Chamran University of Ahvaz, Iran
[d] Young Researchers and Elite Club, Yasooj Branch, Islamic Azad University, Yasooj, Iran
[e] Department of Mechanical and Manufacturing Engineering, Centre for Bioengineering Research and Education, University of Calgary, Calgary, Canada

A B S T R A C T

Due to the instinctive temperature-dependent heat capacity of the Nano-Encapsulated Phase Change Material (NEPCM), there is a growing interest in the potential applications of such materials in heat transfer. As such, steady-state natural convection in a porous enclosure saturated with nanofluid using NEPCMs has been investigated in this study. The cavity is assumed to have constant hot and cold temperatures at the left and right vertical boundaries, respectively, and fully insulated from the bottom and top walls. Considering the Local Thermal Non-equilibrium (LTNE) approach for the porous structure, the governing equations are first non-dimensionalized and then solved by employing the finite element Galerkin method. The impact of different parameters, such as porous thermal conductivity (k_s), solid-fluid interface heat transfer ($10 \leq H \leq 10^5$), Stefan number ($0.2 \leq Ste \leq 1$), and volume fraction of nanoparticles ($0.0 \leq \varphi \leq 0.05$) on the patterns of the fluid and solid isotherms, streamlines and the contours of the heat capacity ratio, fusion temperature ($0.05 \leq \theta_f \leq 1$), local and average Nusselt numbers, and overall heat transfer ratio has been studied. It is shown that improving the porous thermal conductivity not only leads to an increase in the rate of heat transfer but also augments the fluid flow inside the cavity. For low values of the *Ste*, the rate of heat, transferred in the porous enclosure, is intensified. However, regardless of the amount of the Stefan number, the maximum rate of heat transfer is achievable when the non-dimensional fusion temperature is approximately 0.5. Employing NEPCMs in a highly conductive porous structure is more efficacious only when the phases are in the state of local thermal equilibrium. Nonetheless, the rate of heat transfer is higher when the Local thermal non-equilibrium is validated between the phases. Besides, for poor thermal conductivity of the porous medium like glass balls (LTE condition), adding 5% of the nano-encapsulated phase change materials to pure water can boost the rate of heat transfer up to 47% (for $Ste = 0.2$ and $\theta_f = 0.5$). This thermal investigation of NEPCMs shows in detail how advantageous are these nanoparticles in heat transfer and opens up an avenue for further application-based studies.

1. Introduction

Phase Change Materials (PCM), owing to their admirable features in storing and releasing energy during their phase transition, are extensively employed for meticulously managing thermal systems. PCMs are usually employed as reliable agents for cooling the overheating electronic gadgets and controlling thermal processes [1, 2]. Besides, one of the acclaimed application of PCMs is in Thermal Energy Storage (TES) systems. In essence, since the PCMs could release energy when the

surrounding is freezing and absorb energy when melting, they have been extensively employed in thermal energy storage systems and their features have been studied by numerous researchers, both experimentally and numerically.

Nonetheless, knowing the fact that the PCMs have low thermal conductivity by instinct, which extremely affects the thermal performance in thermal energy systems, many investigators have tried to increase the overall thermal performance of the systems implementing several methods, such as using porous metal foams [3, 4, 5, 6], metal matrix [7],

$$\partial T_{nf}/\partial y = \partial T_s/\partial y = 0, \; u=v=0$$

$T_{nf} = T_s = T_h, \; u=v=0$

Heat storage

Heat absorb

Heat release

Porous media

$T_{nf} = T_s = T_c, \; u=v=0$

L

Shell
Core

NEPCM particle

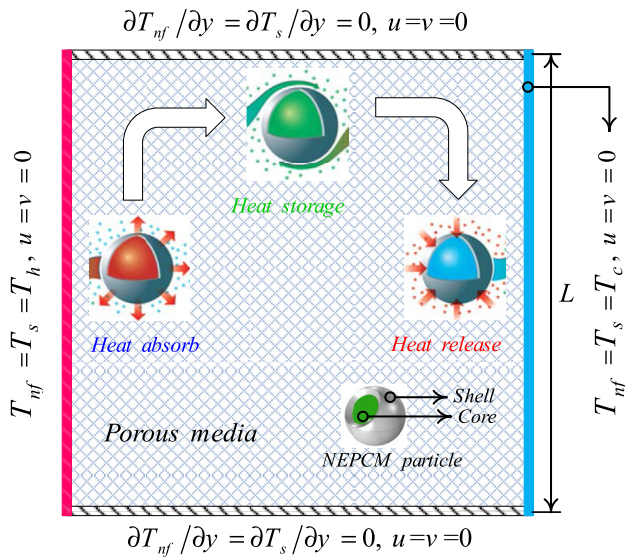$$\partial T_{nf}/\partial y = \partial T_s/\partial y = 0, \; u=v=0$$

Figure 1. Schematic view of the geometry.

fin [8, 9, 10, 11], and nanoparticles dispersed into the PCMs [12, 13, 14, 15], and nano-encapsulation PCMs [16, 17, 18, 19]. Since nanoparticles play a promising role in enhancing the thermal performance of multifarious systems, the mixture of PCM and nanoparticles to produce Nano-enhanced Phase Change Materials (NePCM) has been extensively investigated. In this approach, conventional nanoparticles are dispersed in a phase change material to improve the thermal conductivity of the mixture. The impacts of dispersing the copper nanoparticles in a PCM on its thermophysical properties and the melting/solidification time were studied by Wu et al. [20]. They found that the thermal conductivity of the PCM can be improved up to 14.2% and 18.1% in the solid and liquid phases. The outcomes also presented a reduction in the solidification/melting time by dispersing a 1% mass fraction of the nanoparticles.

According to the experiments of [21], adding nano-sized particles to pure phase change materials alter their rheological properties. Ghalambaz et al. [22], for the first time, using the Power-Law model, studied the impact of rheological properties of the nano-enhanced PCMs on their melting rate and revealed that, owing to the increment of the apparent viscosity, the melting rate remarkably decreases with increasing the volume fraction of nanoparticles. Further, they showed that the rate of heat transfer increases when the melted nano-PCM exhibits shear-thinning behavior (i.e., lower Power-Law index). The also studied

the simultaneous impacts of magneto- and ferro-hydrodynamics on melted volume fraction and melting front of the nano-enhanced PCM and showed that the melted volume fraction increases with the increment of the magnetic parameter and declines when the Hartman number elevates.

The melting phenomenon of the nano-phase change material inside an enclosure, in which aluminum oxide (Al_2O_3) and water are used as nanoparticles and PCMs, is studied in [23]. The outcomes show that mixing nanoparticles with water-PCM enhances the thermal conductivity, melting performance, and viscosity of the nano-PCM; however, as viscosity increases, convection heat transfer decreases. The influence of cyclic melting and solidification of NePCMs based heat sink on managing heat transfer in electronic systems has been studied numerically considering copper oxide (CuO) as nanoparticle and n-Eicosane as PCM [24]. It is shown that the addition of CuO increases the melting rate from 0 to 5%. The decline in the base temperature of the heat sink, down to 4 °C, was observed, which is appropriate for electronic utilization.

The application of nano-PCM in energy storage systems using CuO nanoparticles and cyclohexane PCM, embedded in a porous material, has also investigated numerically [15]. It is shown that when the porosity in the porous medium is small and the volume fraction of nanoparticles is
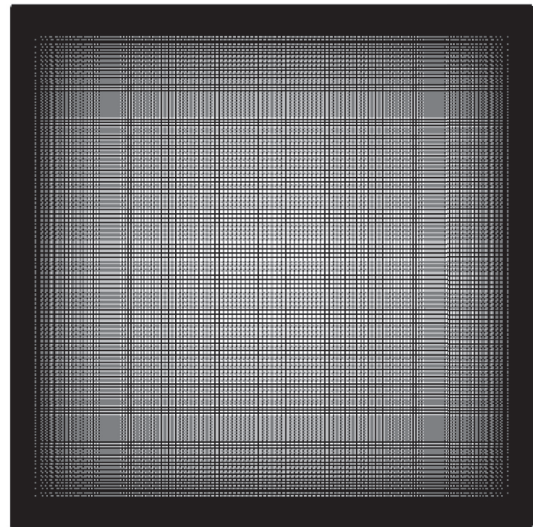

Figure 2. The adopted grid to discretizing the domain; the size of the grid is 200×200 with a stretching ratio of eight.

Table 1. Thermophysical properties of solid matrix and the components of the suspension [31].

Property	ρ (Kgm^{-3})	k (Wm^{-1}K^{-1})	C_p (Jkg^{-1}K^{-1})	μ (kgm^{-1}s^{-1})	β (K^{-1})
Base fluid	997.1	0.613	4179	8.9×10^{-4}	21.0×10^{-5}
Glass balls	2700	1.05	840	-	0.90×10^{-5}
Aluminum foam	2700	205	897	-	2.22×10^{-5}
Cooper foam	8933	400	385	-	1.67×10^{-5}
PU	786	-	1317.7	-	-
Nonadecane	721	-	2037	-	-

Table 2. Dependency of the average Nusselt numbers of fluid and solid phases and the flow strength with grid size ($Ra = 10^7$, $Pr = 6.2$, $Ste = 0.2$, $Nc = 23.8$, $Nv = 12.5$, $Da = 3.1 \times 10^{-4}$, $\theta_f = 0.05$, $\varepsilon = 0.92$, $\varphi = 0.05$, $k_s = 1.05$, $\lambda = 0.32225$ and $H = 100$).

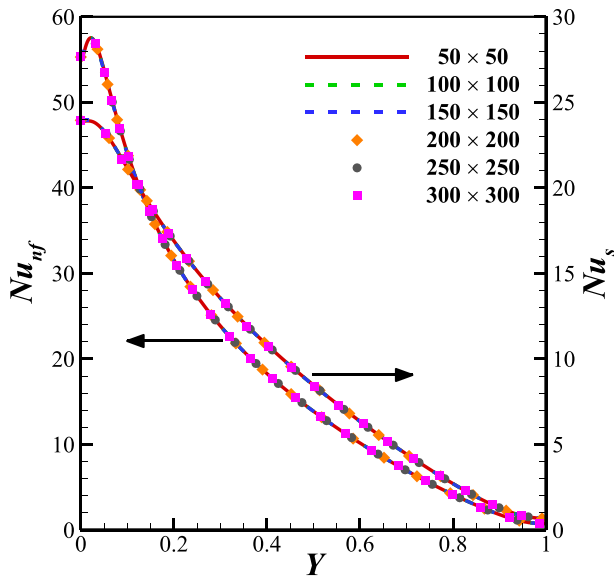| Grid size	50×50	100×100	150×150	200×200	250×250	300×300
Nu_{nf}	18.4252	18.4134	18.4119	18.4108	18.4114	18.4113
Nu_s	9.8124	9.8065	9.8055	9.8049	9.8051	9.8050
ϕ_{max}	29.3192	29.3921	29.4054	29.4117	29.4139	29.4137

Figure 3. Local Nusselt numbers of fluid and solid phases for different grid size ($Ra = 10^7$, $Pr = 6.2$, $Ste = 0.2$, $Nc = 23.8$, $Nv = 12.5$, $Da = 3.1 \times 10^{-4}$, $\theta_f = 0.05$, $\varepsilon = 0.92$, $\varphi = 0.05$, $k_s = 1.05$, $\lambda = 0.322$ and $H = 100$).
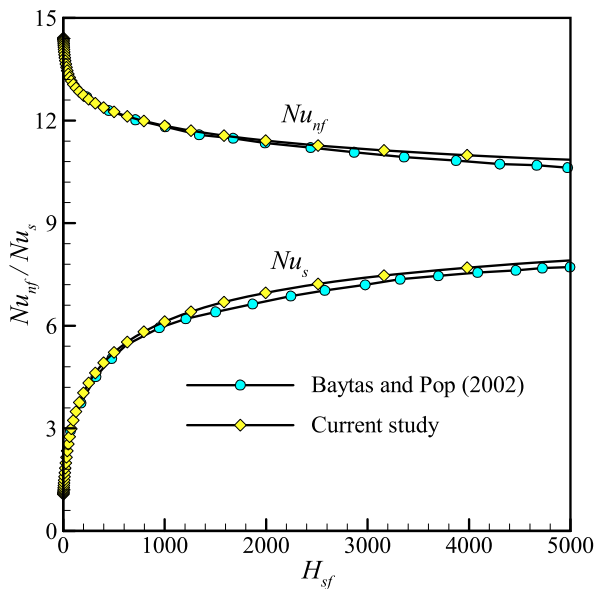

Figure 4. The comparison between Nusselt numbers of fluid and solid phases of the current study and the study conducted by Baytas and Pop [61].

high, the nano-PCM is melted faster. Moreover, the completion of the melting process needs less energy in the higher volume fraction of CuO. Thermal management in electronic components is predicted by employing carbon foam matrix saturated with PCM (Paraffin wax (RT65)) and Multi-Wall Carbon Nano Tubes (MWCNTs) [25]. Thermal conductivity improvement in the carbon foam microcells is observed. A significant decrease in the temperature of electronic equipment was

achieved. Using carbon foam porosities 75% and 88% leads to 11.5% and 7.8% reduction in the surface temperature of electronic components, respectively. Considering n-octadecane paraffin dispersed with Cu nanoparticles, the effect of NePCM melting in partially-filled horizontal elliptical cavities has been investigated [26]. The cavities with different aspect ratios are assumed, and it is concluded that although increasing the nanoparticles-concentration would enhance the melting rate, it causes a decrease in the amount of the phase change materials [26].

Using copper (Cu)/water as nanoparticle/PCM, several researchers investigated the performance of this combination on the solidification of PCMs in the trapezoidal cavity [27], latent heat storage considering wavy surface [28], and thermal energy storage in annuli [29]. In these studies [27, 28, 29], it is shown that the dispersion of nanoparticles in PCM causes a noticeable decrease in solidification or freezing as well as enhancement in heat release. It is found that employing various PCMs with a declining order of melting temperature is more effective in thermal energy storage [30].

Another approach of using phase change materials for energy storage and thermal enhancement is using Nano-Encapsulated Phase Change Materials (NEPCMs). In this approach, the phase change materials are encapsulated in a nanoshell, in the form of a nano-encapsulated phase change particle. Then, these nano-encapsulated phase change particles can be dispersed in a host liquid and produce a suspension. Barlak et al. [31] experimentally studied the dynamic viscosity and thermal conductivity of two different types of suspensions prepared by NEPCMs particles dispersed in ethylene and water as the base fluids. They found the upward and downward tendencies in the viscosity of the suspensions with increases in the volume fraction of NEPCMs particles and temperature, respectively. Also, the thermal conductivity of the suspensions was observed to increase with increasing the volume fraction of NEPCMs particles and temperature.

Considering a suspension of nano-encapsulated phase change materials, there are only a few literature studies. Ghalambaz et al. [32] modeled the free convection of a suspension of NEPCMs in a cavity with temperature difference side-walls. The NEPCM particles circulate in the cavity along with the fluid. When they reach to a hot region with a temperature higher than their fusion temperature, the PCM core of the nanoparticle absorbs the heat and undergoes a phase change process. Accordingly, when the NEPCM particle reaches a cold region below the fusion temperature, the core of the particle releases its latent heat and phase change to solid. The results of [32] indicate about 10% heat transfer enhancement due to the presence of NEPCM particles. The performance of using NEPCMs also depends on the fusion temperature of NEPCMs. Following Ghalambaz et al. [32], Hajjar et al. [33] explored the unsteady heat transfer of NEPCMs in an enclosure-cavity with a time-periodic hot wall temperature. The results of the unsteady-study heat transfer demonstrated a 21% thermal enhancement by using a 2.5% volume fraction of NEPCM particles.

Heat transfer in porous media is widely investigated due to its importance in industry, and different aspects of porous and fluid characteristics have been studied [34, 35, 36, 37]. In fact, in the cases which porous medium thermal conductivity is approximately low or there is high interaction between the base fluid and porous structure, it is entirely reasonable to consider the model of Local Thermal Equilibrium (LTE) for the system in which the temperatures of porous medium and fluid have almost the same value. This assumption simplifies the issue through which the fluid and porous medium can be considered as a uniform mixture. However, there are multiple other cases, mostly when the

Table 3. The average Nusselt number for a clear flow cavity filled with a nanofluid obtained in the present study and those reported by Kahveci [60] when $Nc = 3.3$, $Nv = 2.88$, $Pr = 6.2$, and $Ra = 10^6$.

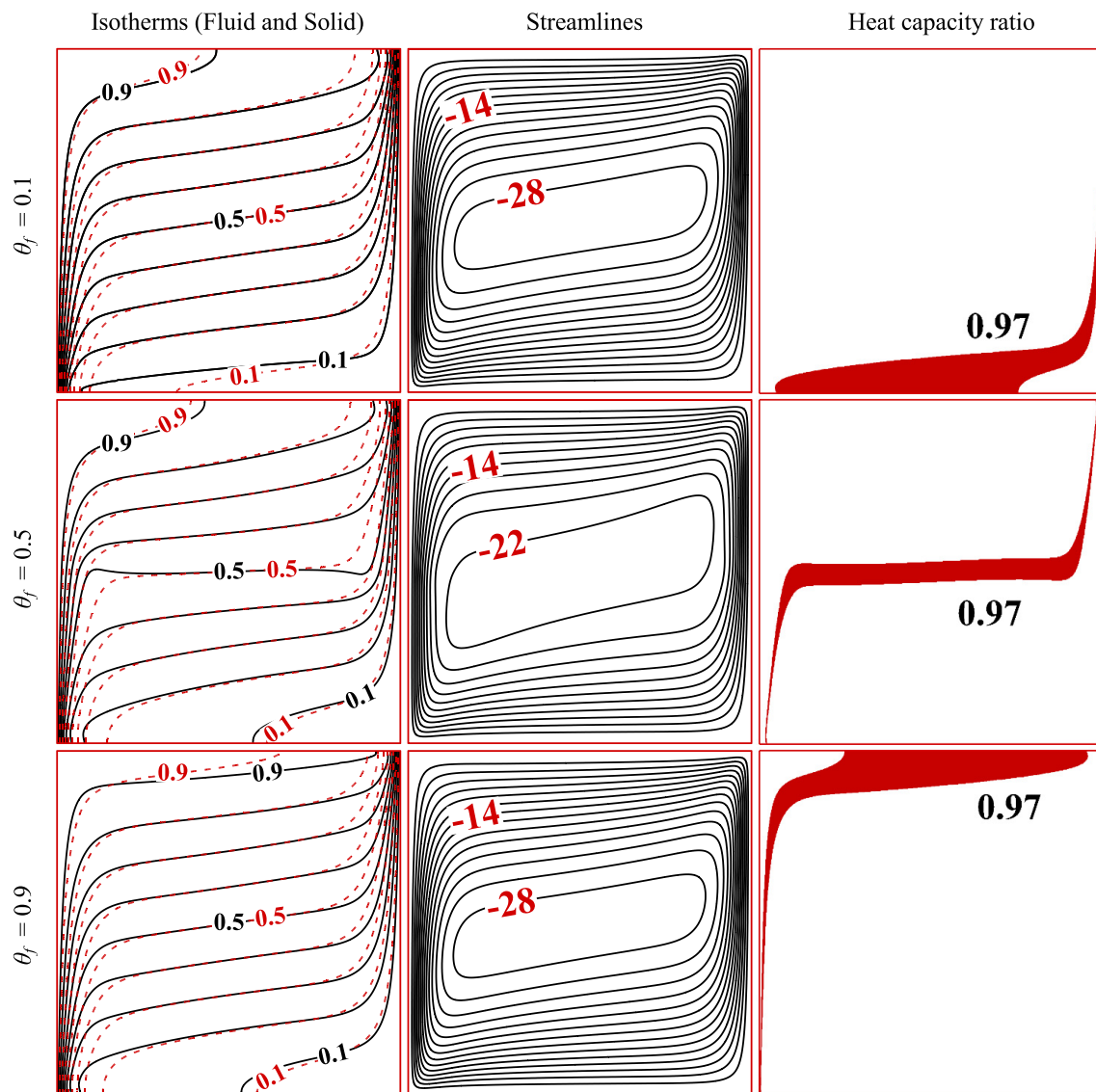| φ	0	0.05	0.1
Current investigation	9.200	9.760	10.300
Kahveci [60]	9.230	9.783	10.297

Figure 5. Influence of the fusion temperature on the isotherms of fluid (solid black lines) and solid (dashed red lines), streamlines, and the contour of heat capacity ratio ($\varphi = 0.05$, $Ste = 0.2$, $k_s = 1.05$ and $H = 100$).

porous is saturated with nanofluid; the temperature of the porous medium is noticeably different from fluid [38, 39, 40, 41, 42]. In this regard, the consideration of LTE is no longer valid and assuming Local Thermal Non-Equilibrium (LTNE) model between the porous and fluid is more rational. Various aspects of LTNE models for regular nanofluids such as conjugate heat transfer [38], hybrid nanofluids [39], partially porous layer (fin) [41], and internal heat generation [43] are investigated in a porous cavity.

Alsabery et al. [38] studied the impacts of the LTNE conditions on the natural convection of the Al_2O_3 nanofluid flowing in a porous medium with the hot bottom wavy bound and a centered non-isothermal cylinder. The heat transfer through the fluid phase was found to increase at high values of porosity by the augmentation of the volume fraction, while an increasing-decreasing tendency was observed at low values of porosity. Mehryan et al. [44] analyzed the free convection of a magnetic hybrid suspension flowing in a double-porous media by utilizing a two-equation energy model. The numerical results showed that an enhancement in the heat transfer rate can be obtained with a decrease in the ratio of the solid-liquid interface convection parameter of the lower layer to the upper one.

Moreover, using NEPCMs, dispersed in the fluid, causes a remarkable difference between the abovementioned temperatures, and consequently, the problem should be solved with LTNE assumption. Considering the heat transfer of NEPCMs in porous media, Ghalambaz et al. [45] studied the mixed convection of NEPCMs in the boundary layer of a vertical flat plate embedded in a porous space. It was assumed that there is a local-thermal equilibrium for the porous medium and NEPCMs suspension. The results show that the presence of NEPCM particles always improves the mixed convection heat transfer. Moreover, the thermal enhancement of using NEPCMs is under a significant influence of the fusion temperature of NEPCM cores. In a very recent study, Ghalambaz et al. [46] theoretically addressed the transient free convection of NEPCMs in a cavity filled with a porous medium using the LTE model. They used the low thermal conductive glass-balls as the porous medium. Due to the low thermal conductivity of the glass-ball porous matrix, the assumption of LTE was justified. However, high thermally conductive metal-foams with the high porosity and the large surface area inside the pores are promising for better heat transfer and fast charging/discharging of NEPCMs.

Regarding the free convection of NEPCMs, Ghalambaz et al. [32] and Hajjar et al. [33] studied the heat transfer of NEPCMs in a clear cavity
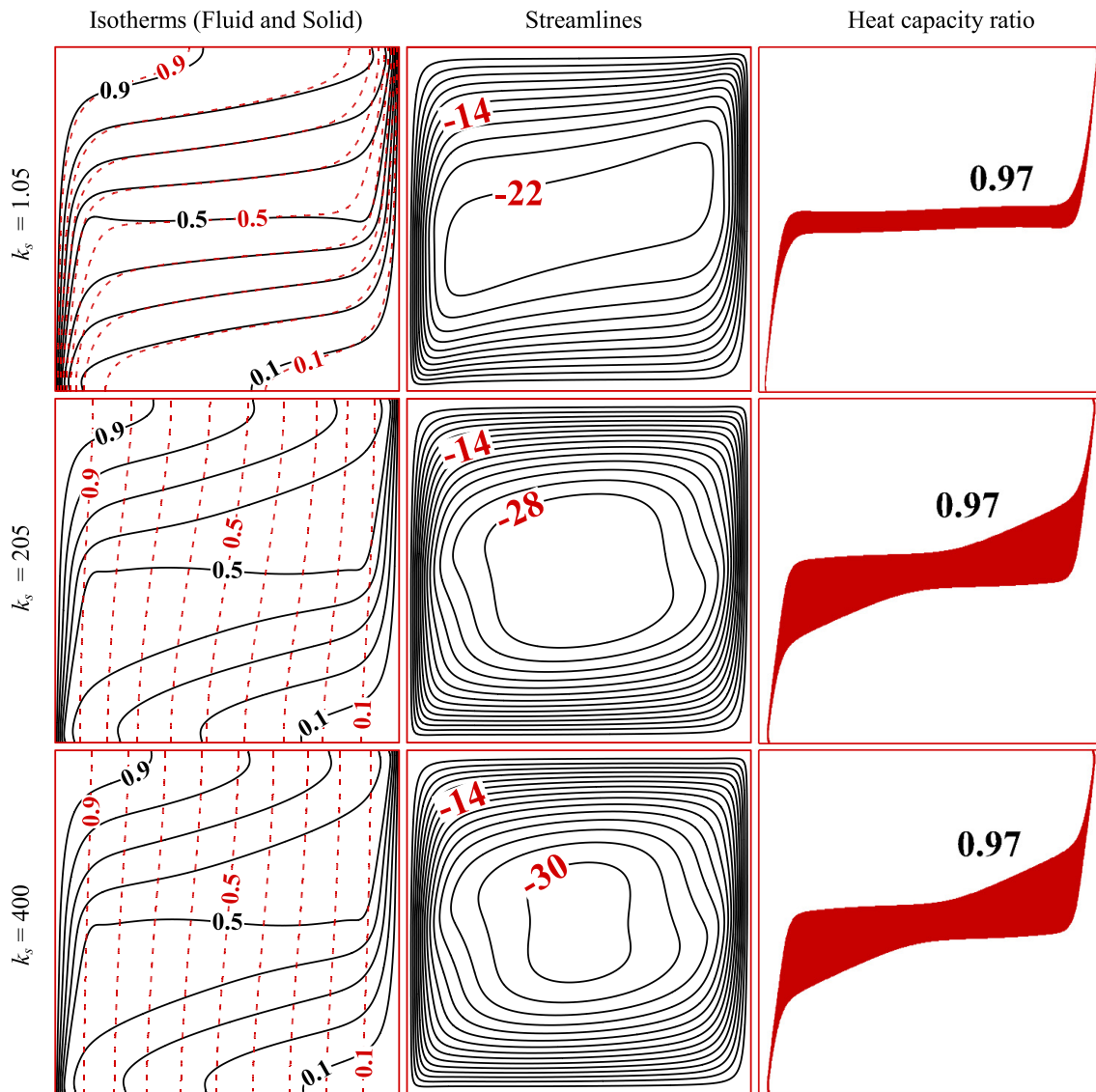
Isotherms (Fluid and Solid)   Streamlines   Heat capacity ratio

Figure 6. Influence of the thermal conductivity of the porous matrix on the isotherms of fluid (solid black lines) and solid (dashed red lines), streamlines, and contour of the heat capacity ratio ($\varphi = 0.05$, $Ste = 0.2$, $k_s = 1.05$ and $H = 100$).

with no porous medium, while Ghalambaz et al. [46] addressed the unsteady heat transfer of NEPCMs in a cavity filled with a porous medium using LTE model. As seen, there are only a few studies regarding the free convection heat transfer of NEPCMs. As mentioned, the LTE model neglects the temperature difference between the porous matrix and the working fluid and is limited to the low thermal conductive porous material. However, the LTNE model, which is the subject of the present research, takes into account the temperature difference between the porous matrix and working fluid by an extra PDE and is capable of modeling high thermally conductive materials such as metal foams. The motivation behind the present work is to investigate free convection of a suspension of NEPCM in a porous cavity by taking into account the LTNE effects.

2. Problem physics

A geometric model of the porous square cavity having the characteristic length of L is demonstrated in Figure 1. The left and right sides of the chamber act as the warm and cold surfaces with the T_h and T_c temperatures. The other bounds are perfectly insulated. The working fluid is a suspension of NEPCM particles and water. The temperatures of the

suspension and the solid matrix are locally different. The energy balance between the components of the porous medium is microscopically established as a result of the LTNE assumption. The NEPCM particles have two parts; phase-change core and shell. The materials making the core and shell are nonadecane and polyurethane (PU). Three different materials are chosen as the solid matrix; glass balls, aluminum, and copper metal foams. The thermophysical properties of the solid matrix and the components of the suspension are tabulated in Table 1.

It is assumed that the temperature differences between the hot wall and the cold wall are limited, so that, the Boussinesq approximation is employed to model the buoyancy forces due to the temperature differences in the fluid. As the flow is natural convection and confined in the porous structure, the flow is considered as laminar. Most of the liquids in typical situations can be regarded as incompressible and Newtonian. The NEPCM suspension remains uniform, and the surface of the porous matrix is treated to prevent the sedimentation or filtration of NEPCM particles. The NEPCMs are also treated by charge methods or additives to prevent agglomeration. The porous medium is saturated with the liquid, and there is no capillary effect. The source of convection heat transfer is a temperature difference. Finally, the temperature difference between the porous matrix and the liquid inside the pores is taken into account, which
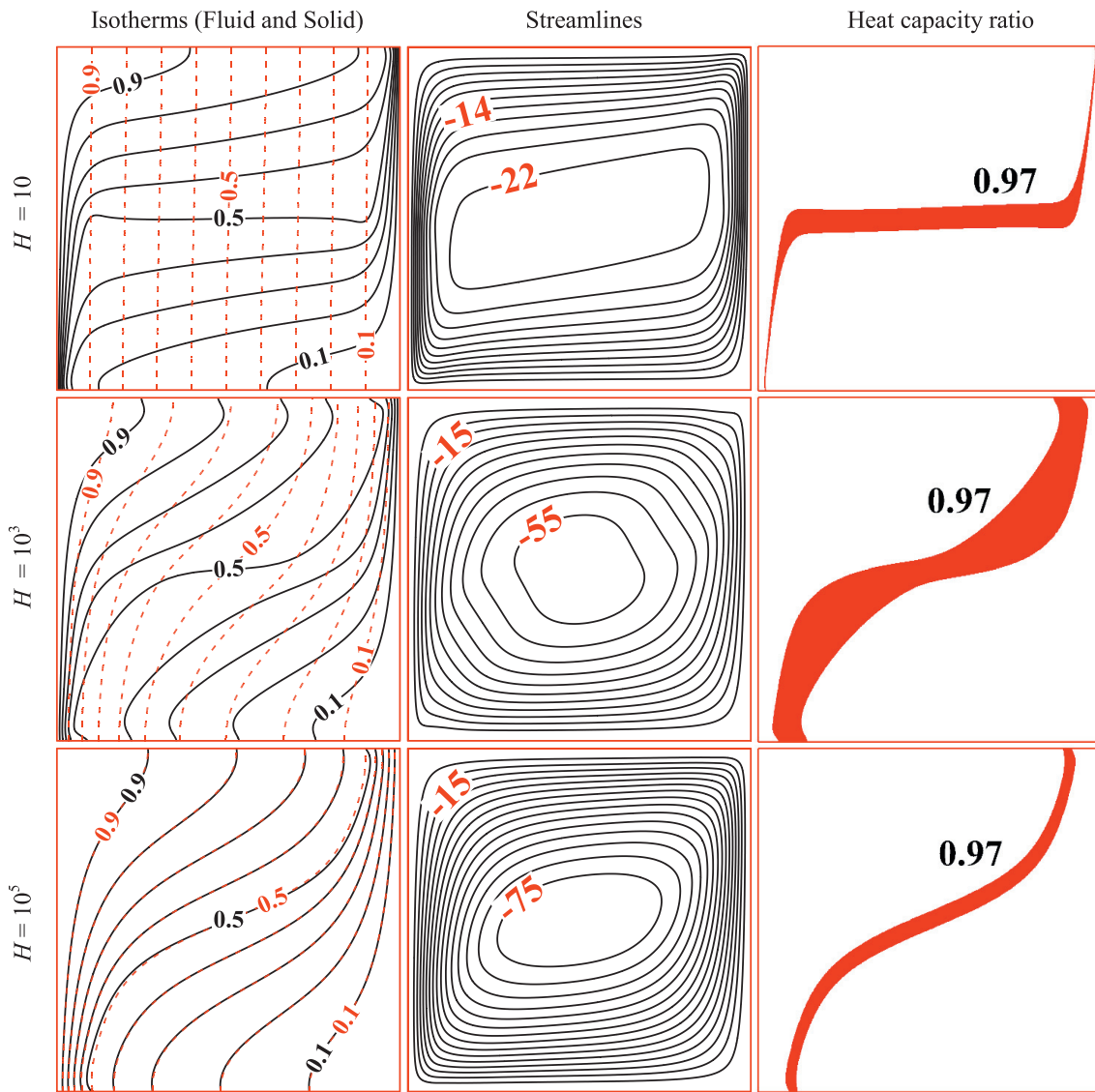
Isotherms (Fluid and Solid)   Streamlines   Heat capacity ratio

Figure 7. Influence of the thermal conductivity of the porous matrix on the isotherms of fluid (solid black lines) and solid (dashed red lines), streamlines and contour of the heat capacity ratio ($\varphi = 0.05$, $Ste = 0.2$, $k_s = 205$ and $\theta_f = 0.5$).

led to the LTNE model. Invoking the mentioned assumptions, the governing equations for the steady-state, laminar and incompressible fluid flow and LTNE heat transfer in porous medium and liquid inside the porous medium are introduced. Here, following the standard equation of Darcy Brinkman model for flow and LTNE model for heat transfer of a liquid [47], the governing equations of the fluid and solid are:

$$\frac{\partial u}{\partial x} + \frac{\partial v}{\partial y} = 0 \tag{1}$$

$$\frac{\rho_{nf}}{\varepsilon^2}\left(u\frac{\partial u}{\partial x} + v\frac{\partial u}{\partial y}\right) = -\frac{\partial p}{\partial x} + \frac{\mu_{nf}}{\varepsilon}\left(\frac{\partial^2 u}{\partial x^2} + \frac{\partial^2 u}{\partial y^2}\right) - \frac{\mu_{nf}}{\kappa}u \tag{2}$$

$$\frac{\rho_{nf}}{\varepsilon^2}\left(u\frac{\partial v}{\partial x} + v\frac{\partial v}{\partial y}\right) = -\frac{\partial p}{\partial y} + \frac{\mu_{nf}}{\varepsilon}\left(\frac{\partial^2 v}{\partial x^2} + \frac{\partial^2 v}{\partial y^2}\right) + g\rho_{nf}\beta_{nf}\left(T_{nf} - T_c\right) - \frac{\mu_{nf}}{\kappa}v \tag{3}$$

$$\left(\rho C_p\right)_{nf}\left(u\frac{\partial T_{nf}}{\partial x} + v\frac{\partial T_{nf}}{\partial y}\right) = \varepsilon k_{nf}\left(\frac{\partial^2 T_{nf}}{\partial x^2} + \frac{\partial^2 T_{nf}}{\partial y^2}\right) + h\left(T_s - T_{nf}\right) \tag{4}$$

$$0 = (1-\varepsilon)k_s\left(\frac{\partial^2 T_s}{\partial x^2} + \frac{\partial^2 T_s}{\partial y^2}\right) + h\left(T_{nf} - T_s\right) \tag{5}$$

The boundary conditions in the mathematical form are as follows:

$$\forall\, x,\, y \mid x = 0,\, 0 \leq y \leq L \Rightarrow u = v = 0,\ T_{nf} = T_s = T_h \tag{6}$$

$$\forall\, x,\, y \mid x = L,\, 0 \leq y \leq L \Rightarrow u = v = 0,\ T_{nf} = T_s = T_c \tag{7}$$

in which the velocities at the walls are zero, and the temperatures at the right and left walls are isothermal with hot and cold temperatures of T_h and T_c, respectively.

$$\forall\, x,\, y \left|\begin{array}{l} y = 0,\ 0 \leq x \leq L \Rightarrow u = v = 0,\ \dfrac{\partial T_{nf}}{\partial y} = \dfrac{\partial T_s}{\partial y} = 0 \\[2mm] y = L,\ 0 \leq x \leq L \Rightarrow u = v = 0,\ \dfrac{\partial T_{nf}}{\partial y} = \dfrac{\partial T_s}{\partial y} = 0 \end{array}\right. \tag{8}$$

In the above equation, the top and bottom walls are impermeable, with zero velocity and adiabatic.

Isotherms (Fluid and Solid)   Streamlines   Heat capacity ratio
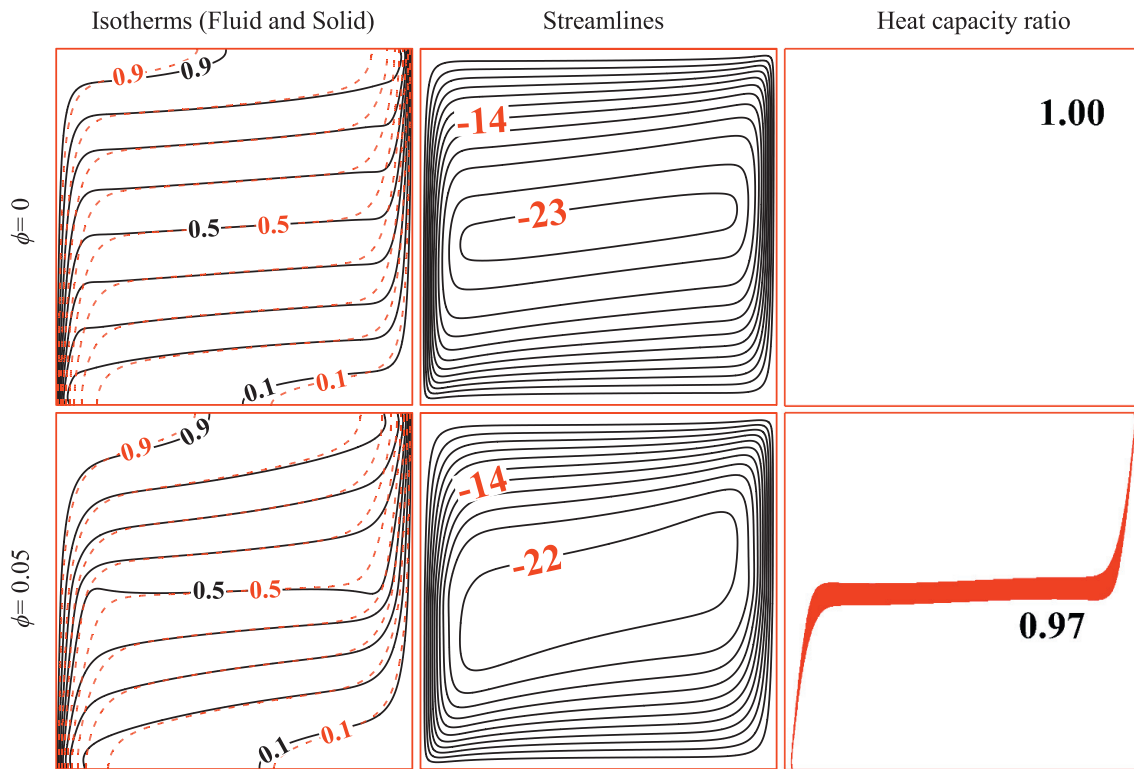

Figure 8. Influence of the NEPCMs' volume fraction on the isotherms of fluid (solid black lines) and solid (dashed red lines), streamlines and contour of the heat capacity ratio ($Ste = 0.2$, $k_s = 205$ and $\theta_f = 0.5$).
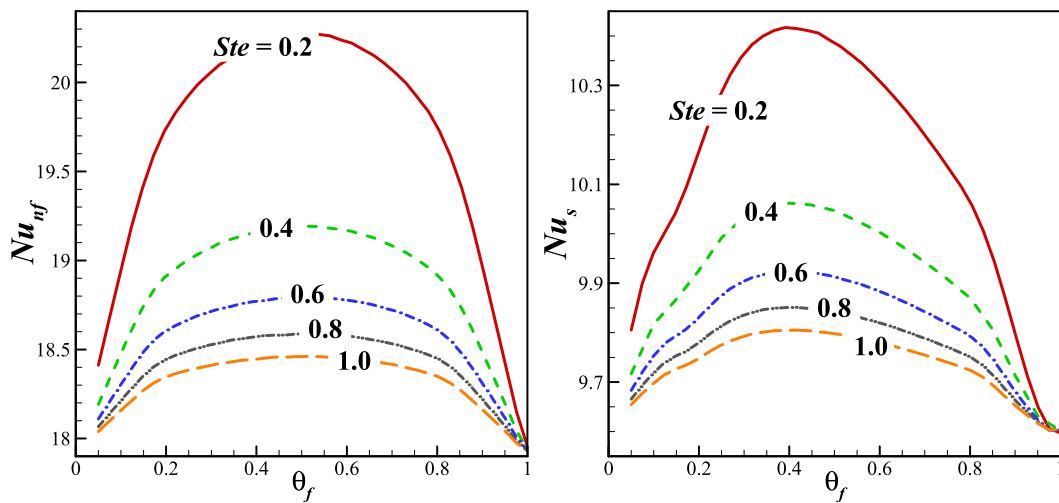

Figure 9. Variation of the average Nusselt numbers of the fluid (left) and the solid matrix (right) with the fusion temperature and the Stefan number ($\varphi = 0.05$, $k_s = 1.05$ and $H = 100$).

2.1. Suspension bulk properties

The suspension is a mixture of NEPCM particles and the working fluid; hence, the following equations are utilized to demine the effective values of the thermophysical properties. The following weighted function is employed for achieving the density of suspension [48]:

$$\rho_{nf} = (1 - \varphi)\rho_{bf} + \varphi\rho_p \tag{9}$$

In which the density of NEPCM particles is [48]:

$$\rho_p = \frac{(1 + \chi)\rho_{co}\rho_{sh}}{\rho_{sh} + \chi\rho_{co}} \tag{10}$$

where χ is the weight ratio of core to shell. The following weighted function is employed to obtain the heat capacity of the suspension [49, 50]:

$$C_{p,\,nf} = \frac{(\rho C_p)_{p,eff}\varphi + (\rho C_p)_{bf}(1 - \varphi)}{\rho_{nf}} \tag{11}$$

where the effective specific heat of nano-encapsulated particles, i.e. $C_{p,p,eff}$, without phase change is [48]:
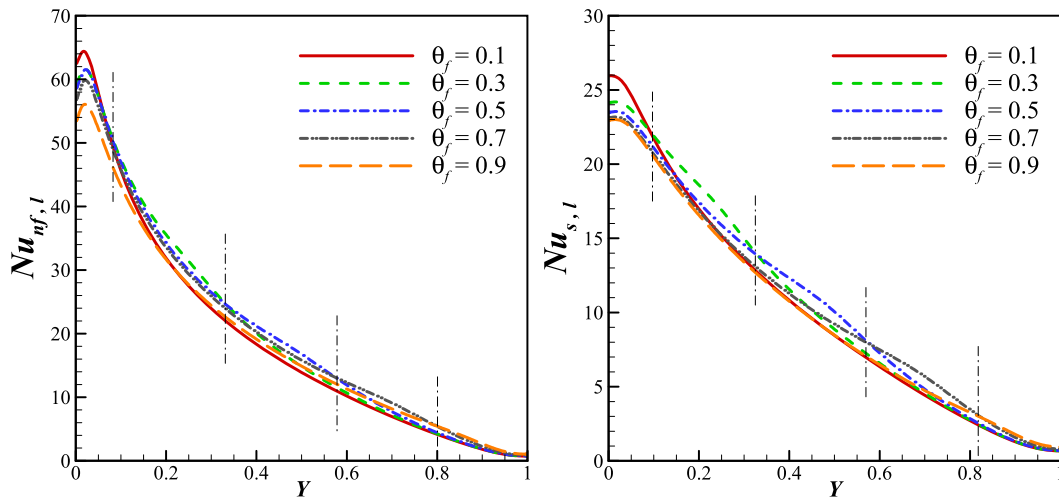
Figure 10. Impact of fusion temperature on the local values of the Nusselt numbers of the fluid (left) and the solid phase (right) ($\varphi = 0.05$, $Ste = 0.2$, $k_s = 1.05$ and $H = 100$).

$$(\rho C_p)_p = \frac{(C_{p,\,co} + \chi C_{p,\,sh})\rho_{co}\rho_{sh}}{(\rho_{sh} + \chi\rho_{co})} \tag{12}$$

If the core of the nanoparticles undergoes a phase change, which this phase change is included in the heat capacity as [32].

$$C_{p,\,p,\,eff} = C_{p,\,p}\left\{\frac{\pi}{2}\cdot\left(\frac{h_{sf}}{T_{Mr}} - C_{p,\,p}\right)\cdot\sin\left(\pi\frac{T_{nf} - T_0}{T_{Mr}}\right)\right\}\begin{cases}0 & T_{nf} < T_0 \\ 1 & T_0 < T_{nf} < T_1 \\ 0 & T_{nf} > T_1\end{cases} \tag{13}$$

T_0 and T_1 are respectively, the lower and upper limits of melting range T_{Mr}:

$$\begin{cases}T_0 = T_f - T_{Mr}/2 \\ T_1 = T_f\ T_{Mr}/2\end{cases} \tag{14}$$

Therefore, the heat capacity of the NEPCM particles consists of two parts, the first part is the regular constant heat capacity, and the second part is the latent heat which is modeled in the term of temperature-dependent heat capacity with an energy absorption similar to the amount of latent heat. The coefficient of thermal volume-expansion for the NEPCM-suspension is as follows [16]:

$$\beta_{nf} = (1 - \varphi)\beta_{bf} + \varphi\beta_p \tag{15}$$

The presence of NEPCM particles changes the dynamic viscosity and thermal conductivity of the suspension. Thus, the following linear functions can be used to obtain the dynamic viscosity and thermal conductivity of NEPCM-suspension [51, 52]:

$$\mu_{nf} = \mu_{bf}(1 + Nv\varphi) \tag{16}$$

$$k_{nf} = k_{bf}(1 + Nc\varphi) \tag{17}$$

Nv and Nc denote the numbers of dynamic viscosity and thermal conductivity. A linear relation for dynamic viscosity and thermal conductivity of nanofluids was proposed by benchmark studies of Buongiorno et al. [53] and Venerus et al. [54]. This relation later was discussed and utilized in the study or Zaraki et al. [51] for nanofluids, and the studies of Ghalambaz et al. [13, 55] for hybrid nanofluids and nano-enhanced PCMs.

2.2. Non-dimensionalizing the equations and boundary conditions

Non-dimensionalization techniques facilitate the study of the problem at hand and lessen the number of free parameters. In the non-dimensionalization technique, an appropriate combination of the fluid properties and flow characteristics needs to be found. The following dimensionless parameters are employed to non-dimensionalize the equations and boundary conditions:

$$X = \frac{x}{L}, \quad Y = \frac{y}{L}, \quad U = \frac{uL}{\alpha_{bf}}, \quad V = \frac{vL}{\alpha_{bf}}, \quad P = \frac{pL^2}{\rho_{bf}\alpha_{bf}^2},$$
$$\theta_{nf} = \frac{T_{nf} - T_c}{\Delta T}, \quad \theta_s = \frac{T_s - T_c}{\Delta T} \tag{18}$$

where $\Delta T = T_h - T_c$. Invoking the non-dimensional parameters, the non-dimensional form of the governing equations is then achieved as:

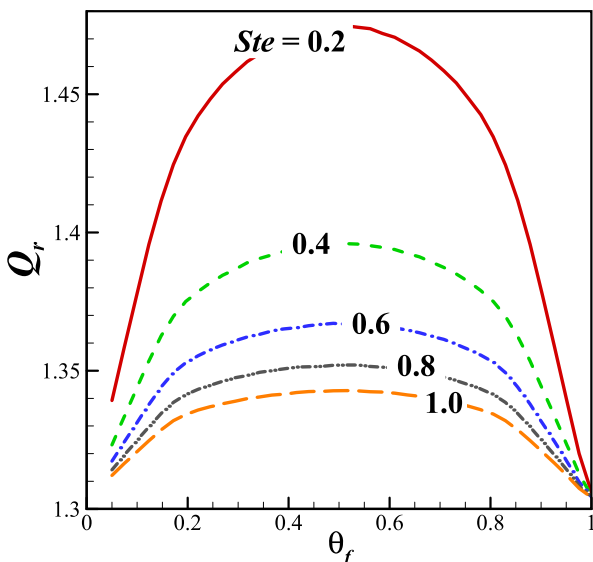$$\frac{\partial U}{\partial X} + \frac{\partial V}{\partial Y} = 0 \tag{19}$$

Figure 11. Variation of the total heat transfer ratio with the fusion temperature and the Stefan number ($\varphi = 0.05$, $k_s = 1.05$ and $H = 100$).
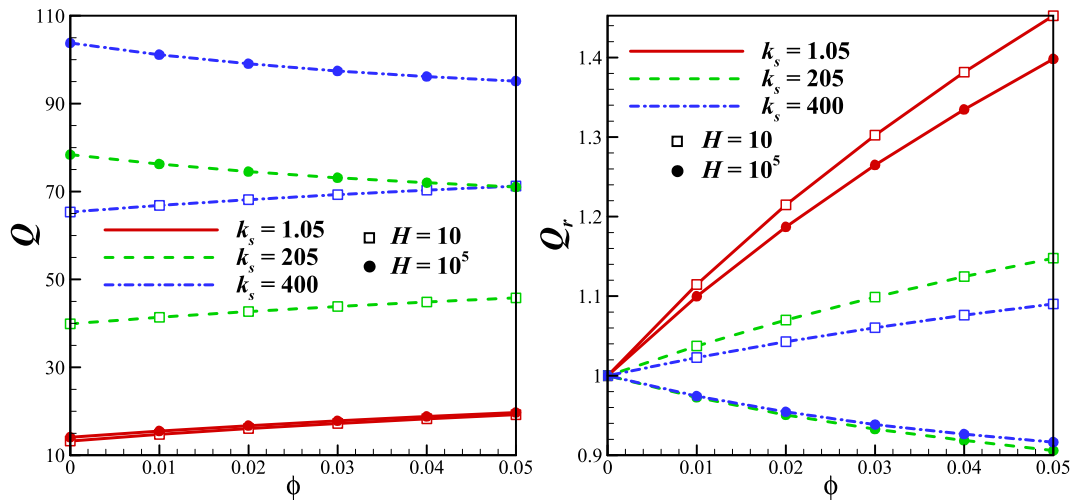
Figure 12. Variation of the total heat transfer (left) and total heat transfer ratio (right) with the volume fraction of NEPCMs, interface heat transfer parameter and the thermal conductivity of the porous matrix ($Ste = 0.2$ and $\theta_f = 0.5$).

Figure 13. Variation of average Nusselt number for the suspension (left) and solid phase (right) with the volume fraction of NEPCMs, interface heat transfer parameter and the thermal conductivity of the porous matrix ($Ste = 0.2$ and $\theta_f = 0.5$).
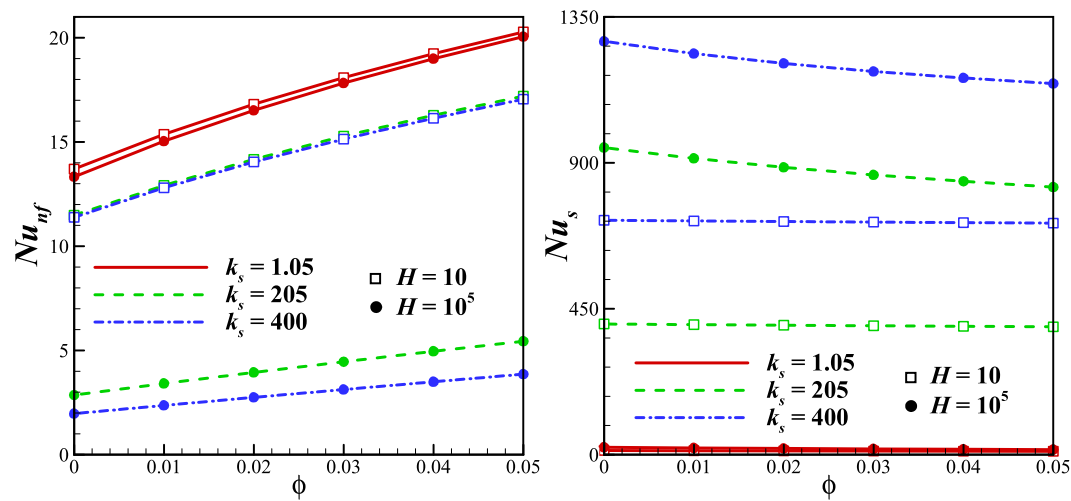
$$\varepsilon^{-2}\left(\frac{\rho_{nf}}{\rho_{bf}}\right)\left(U\frac{\partial U}{\partial X}+V\frac{\partial U}{\partial Y}\right)=-\frac{\partial P}{\partial X}+Pr\varepsilon^{-1}\left(\frac{\mu_{nf}}{\mu_{bf}}\right)\left(\frac{\partial^2 U}{\partial X^2}+\frac{\partial^2 U}{\partial Y^2}\right)$$
$$-\frac{Pr}{Da}\left(\frac{\mu_{nf}}{\mu_{bf}}\right)u \tag{20}$$

$$\varepsilon^{-2}\left(\frac{\rho_{nf}}{\rho_{bf}}\right)\left(U\frac{\partial V}{\partial X}+V\frac{\partial V}{\partial Y}\right)=-\frac{\partial P}{\partial Y}+Pr\varepsilon^{-1}\left(\frac{\mu_{nf}}{\mu_{bf}}\right)\left(\frac{\partial^2 V}{\partial X^2}+\frac{\partial^2 V}{\partial Y^2}\right)$$
$$+Ra\cdot Pr\left(\frac{\beta_{nf}}{\beta_{bf}}\right)\left(\frac{\rho_{nf}}{\rho_{bf}}\right)\theta_{nf}-\frac{Pr}{Da}\left(\frac{\mu_{nf}}{\mu_{bf}}\right)v \tag{21}$$

The parameters appeared in the non-dimensional Eqs. (20) and (21), Rayleigh Ra, Prandtl Pr and Darcy Da numbers, are:

$$Ra=\frac{g\rho_{bf}\beta_{bf}\Delta TL^3}{\alpha_{bf}\mu_{bf}},\ Pr=\frac{\mu_{bf}}{\rho_{bf}\alpha_{bf}},\ Da=\frac{\kappa}{L^2} \tag{22}$$

$$Cr\left(U\frac{\partial\theta_{nf}}{\partial X}+V\frac{\partial\theta_{nf}}{\partial Y}\right)=\varepsilon\left(\frac{k_{nf}}{k_{bf}}\right)\left(\frac{\partial^2\theta_{nf}}{\partial X^2}+\frac{\partial^2\theta_{nf}}{\partial Y^2}\right)+H(\theta_s-\theta_{nf}) \tag{23}$$

where

$$Cr=\frac{(\rho C_P)_{nf}}{(\rho C_P)_{bf}}=(1-\varphi)+\varphi\lambda+\frac{\varphi}{\delta\,Ste}f \tag{24}$$

λ, δ and Ste of the above relations, respectively, are:

$$\lambda=\frac{(C_{p,\,co}+\chi C_{p,\,sh})\rho_{co}\rho_{sh}}{(\rho C_P)_{bf}(\rho_{sh}+\chi\rho_{co})},\ \delta=\frac{T_{Mr}}{\Delta T},\ Ste=\frac{(\rho C_P)_{bf}\Delta T(\rho_{sh}+\iota\rho_{co})}{(h_{sf}\rho_{co}\rho_{sh})} \tag{25}$$

f of Eq. 25, the dimensionless fusion function, can be obtained by substituting the non-dimension form of the parameters into Eq. 13. After some simplifications, it reads

$$f=\frac{\pi}{2}sin\left(\frac{\pi}{\delta}\left(\theta-\theta_f+\frac{\delta}{2}\right)\right)\times\begin{cases}1 & |\theta-\theta_f|\leq\delta/2\\0 & |\theta-\theta_f|\geq\delta/2\end{cases} \tag{26}$$

The dimensionless melting point of the core of NEPCM particles, i.e., θ_f, is:

$$\theta_f=\frac{T_f-T_c}{T_h-T_c} \tag{27}$$

The energy balance equation for the solid matrix in the dimensionless coordinates can be written as follows:

$$0 = (1-\varepsilon)\left(\frac{k_s}{k_{bf}}\right)\left(\frac{\partial^2\theta_s}{\partial X^2} + \frac{\partial^2\theta_s}{\partial Y^2}\right) + H(\theta_{nf} - \theta_s) \tag{28}$$

The dimensionless parameter of H, called the fluid-solid interface heat transfer parameter, is:

$$H = \frac{hL^2}{k_{bf}} \tag{29}$$

Substituting the scales, the boundary conditions in the dimensionless form acquired are:

$$\forall X,\ Y\ |\ X = 0, 0 \le Y \le 1 \Rightarrow U = V = 0,\ \theta_{nf} = \theta_s = 1 \tag{30}$$

$$\forall\ X,\ Y\ |\ X = 1,\ 0 \le Y \le 1 \Rightarrow U = V = 0,\ \theta_{nf} = \theta_s = 0 \tag{31}$$

$$\forall X,Y\ \begin{vmatrix} Y = 0,\ \ 0 \le X \le 1 \Rightarrow U = V = 0,\ \dfrac{\partial\theta_{nf}}{\partial Y} = \dfrac{\partial\theta_s}{\partial Y} = 0 \\[2mm] Y = 1,\ 0 \le X \le 1 \Rightarrow U = V = 0,\ \dfrac{\partial\theta_{nf}}{\partial Y} = \dfrac{\partial\theta_s}{\partial Y} = 0 \end{vmatrix} \tag{32}$$

2.3. Heat transfer rates

The average Nusselt numbers for the fluid and solid phases are determined as the following:

$$Nu_{nf} = \left(\frac{k_{nf}}{k_{bf}}\right)\int_0^L \left(\frac{\partial\theta_{nf}}{\partial X}\right) dY \tag{33}$$

$$Nu_s = \left(\frac{k_s}{k_{bf}}\right)\int_0^L \left(\frac{\partial\theta_s}{\partial X}\right) dY \tag{34}$$

The weighted combination of the Nusselt numbers of fluid and solid phases results in the total heat transfer, i.e., q_{nf}:

$$q_{nf} = \varepsilon k_{nf}\int_0^L \left(\frac{\partial\theta_{nf}}{\partial X}\right) dY + k_s(1-\varepsilon)\int_0^L \left(\frac{\partial\theta_s}{\partial X}\right) dY \tag{35}$$

or

$$Q_{nf} = \frac{q_{nf}}{k_{bf}L} = \varepsilon Nu_{nf} + (1-\varepsilon)Nu_s \tag{36}$$

Q_r is the total heat transfer ratio and shows the total enhancement or deterioration of the heat transfer rate while using NEPCMs.

$$Q_r = \frac{Q_{nf}}{Q_{nf}\big|_{\varphi=0}} = \frac{\varepsilon Nu_{nf} + (1-\varepsilon)Nu_s}{(\varepsilon Nu_{nf} + (1-\varepsilon)Nu_s)_{\varphi=0}} \tag{37}$$

3. Numerical analysis and grid verification

The non-dimensional, nonlinear, and coupled governing equations are solved by employing the finite element method. For this purpose, the equations of (19), (20), (21), (23 and (28) and their corresponding boundary conditions are first rewritten in the weak form and the discretized utilizing the Galerkin method. Using the weak form of the equation, the residual equations are achieved by performing integration over the domain of the solution. Then, the Newton method is applied to iteratively solve the set of algebraic residual equations by employing the PARallel DIrect SOlver (PARDISO) solver [56, 57, 58]. A residual error O (10^{-6}) and a damping factor of 0.8 are utilized for the solution.

The damped Newton method, along with the Parallel Sparse Direct Solver is implemented to solve the set of equations, algebraically. The stopping criteria of 10^{-5} are used for residuals to stop the computations. The details of this method are discussed in [59]. A structured non-uniform grid with regular quadrilateral elements and the variable stretching ratio is employed to discretize the domain. Theoretically, the stretching approach allows producing a dense computational grid with

high resolution wherever it is required, especially in the vicinity of solid boundaries to capture the sharp variation of fluid behaviors. In the present study, as can be seen from its schematic view in Figure 2, a stretched grid with symmetrical distribution on both X and Y directions, and a stretching factor of eight was generated.

Table 2 shows the average Nusselt numbers of the fluid and solid matrix as well as the maximum value of the flow strength in the enclosure for five grid sizes, wherein the experimental data of [31] are used for some of the parameters. As observed, the evaluated parameters show to be independent of the grid size and their maximum variations are less than 1% between coarsest and finest utilized grids. Thus, for further assessment, the graphs of the local Nusselt numbers of the fluid (on the left vertical axis) and the solid (on the right vertical axis) on the hot wall are depicted in Figure 3. As seen, the grid size of 200×200 shows satisfying accuracy and thus is acceptable to be used for simulations.

In a numerical study, the accuracy of the results needs to be confirmed. Hence, the outcomes of the present investigation are compared with several studies published in the literature [60, 61]. Table 3 illustrates the comparison between the heat transfer rates of the current research and those reported by Kahveci [60]. The geometry of the square enclosure and the applied boundary conditions in the work of Kahveci [60] are quite similar to the present one. The enclosure is filled with a nanofluid in which the dynamic viscosity and thermal conductivity numbers were respectively 2.88 and 3.3. Clearly, a quite satisfactory agreement between the outcomes of Kahveci [60] and ours can be found. The comparison has been done for $Nc = 3.3$, $Nv = 2.88$, $Pr = 6.2$, and $Ra = 10^6$.

The results of the present work are further verified for the heat transfer rates through fluid and solid phases of a fluid-saturated porous medium enclosed in this paper with those presented by Baytas and Pop [61] wherein, the LTNE condition was taken into account. The porous medium enclosed was a square enclosure with a left hot and a right cold wall. However, the upper and lower walls are adiabatic. The comparison between the rates of heat transfer through the solid and fluid phases between the results of the current work and the results presented by Baytas and Pop [61] are conducted for different values of modified solid-fluid interface heat transfer parameter ($H_m = H/\varepsilon$), as depicted in Figure 4. In this validation, $Ra \times Da = 10^3$. Further, the value of the modified thermal conductivity ratio, $K_r = \varepsilon k_{bf}/(k_s - \varepsilon k_s)$, is 10. As can be seen from Figure 4, excellent matching can be observed.

4. Outcomes and discussion

Herein, the impacts of different involved parameters on the flow and thermal fields of the suspensions comprising NEPCMS are analyzed. These parameters are as follows: Stefan number ($0.2 \le Ste \le 1$), solid-fluid interface heat transfer parameter ($10 \le H \le 10^5$), dimensionless fusion-temperature ($0.05 \le \theta_f \le 1$), volume fraction of the NEPCMs ($0.0 \le \varphi \le 0.05$), material of the solid matrix ($k_s = 1.05$, 205 and 400 W/m. K). Here the conductivity and viscosity numbers are adopted as $Nc = 23.8$, $Nv = 12.5$. Furthermore, water ($Pr = 6.2$) is considered as the base fluid. Besides, the values of the Darcy number, porosity of the porous medium, the ratio of the heat capacity of the NEPCM particles to the base liquid, and the Rayleigh number are considered to be constant at 3.1×10^{-4}, 0.92, 0.32, and 10^7, respectively.

The contours of the fluid and solid temperatures, streamlines, and heat capacity ratio are depicted in Figure 5. The red ribbons in the Cr contours show the regions that the NEPCMs undergo a phase change, and thus, the heat capacity increased. In fact, the PCMs in the capsules can be found in three states: pure solid, pure liquid, or during the phase transition. The first two cases are treated as simple nanoparticles with no specific feature or impact on the heat capacity (see Eq. (12) for these cases). On the other hand, wherever the fluid temperature is around the fusion temperature of the NEPCMs, or in other words, whenever phase change occurs in the capsulated PCMs, an extra heat needs to be absorbed

by these capsules to proceed the phase transition. A temperature-dependent term models this additional latent heat in the heat capacity. In other terms, the red ribbons depict the region where the PCMs in the capsules are partially melted. Note that the heat capacity ratio is identical to 0.966 wherever no phase change occurs inside capsules and the contour presents the level 0.97. It can be seen that for each fusion temperature, the red ribbon is developed around the corresponding isotherm. It is worth mentioning that the heat capacity ratio approach to its maximum, which is about four or higher, precisely on its equivalent isothermal line.

The patterns of the streamlines and isotherms of the fluid and solid is more affected for $\theta_f = 0.5$, and the flow strength is lower than the cases $\theta_f = 0.1$ and 0.9. This can be explained by the fact that the fluid temperature remains approximately constant during the phase change (i. e. on the red ribbon), resulting in the reduction of the buoyancy force and thus the decline of the fluid flow. The average value of the heat capacity for $\theta_f = 0.5$ over the entire domain is $\int \int Cr\, dA = 1.2622$, while for the cases of $\theta_f = 0.1$ and 0.9 is equal and identical to $\int \int Cr\, dA = 1.4368$. This means for that $\theta_f = 0.5$, the phase change occurs in more capsules, or in other words, the fluid temperature is almost constant in a larger area, and thus, the fluid flow for this case is minimum.

Figure 6 illustrates the impact of the porous medium thermal-conductivity on the patterns of the fluid and solid isotherms, streamlines, and the contours of Cr. Increasing thermal-conductivity of the solid-matrix boosts the conduction mechanism and thus the heat transfer is intensified, resulting in higher fluid flow in the cavity. Moreover, the solid isotherms are almost vertical for higher k_s, indicating that the conduction heat transfer prevails for the solid matrix. A comparison between the solid isotherms reveals that for higher values of the k_s, thermal equilibrium only can be achieved in higher values of the solid-fluid interface heat transfer parameter. The red ribbons in which the phase change occurs for capsules enlarge by increasing the thermal conductivity of the porous medium specifying that more capsules are engaged in the melting process due to thermal-conductivity augmentation.

The effect of the solid-fluid heat transfer parameter of the interface (H) on the patterns of the fluid and solid isotherms, streamlines, and the heat capacity ratio contours is presented in Figure 7. The solid-fluid heat transfer parameter of the interface (H) indicates the pore-scale convective heat transfer between the solid matrix of a porous medium and the liquid inside the pores. Thus is a measure of microscopic heat exchange between the phases. For low values of the heat transfer parameter ($H = 10$), the non-equilibrium effect is considerable, resulting in significant discrepancies between the fluid and solid temperature fields. Increasing the H parameter brings the isotherms of solid and fluid phases closer to each other. While the fluid isotherms slightly move away from the side walls by increasing the heat transfer parameter, specifying a reduction in the rate of fluid heat transfer, the solid ones get closer to the hot and cold walls, indicating an increase in the rate of solid heat transfer. For high values of the H parameter, the temperature isolines of fluid and solid are coincided, indicating that the phases are in the state of the thermal equilibrium. As seen, the flow strength is increased with augmentation of the H parameter. The red ribbons in the contours of Cr enlarge and widens as the H elevates from 10 to 10^3 and then narrows as H increases to 10^5.

The influence of the volume fraction of the nano-encapsulated PCMs on the patterns of the fluid and solid isotherms, streamlines, and the contours of Cr, is presented in Figure 8. As seen, the flow strength decreases marginally due to the augmentation of the nanofluid viscosity (see Eq. 16). Moreover, the isotherms of solid and fluid move lightly away from the sidewalls, indicating a slight decrease in the temperature gradient. On the other hand, adding NEPCMs to the host fluid raises the thermal-conductivity (Eq. 17) and the heat capacity of the nanofluid (Eq. 23), which can compensate the fluid temperature gradient reduction and consequently results in the amplification of the heat transfer rate. In

addition to this, for the case of pure fluid ($\varphi = 0$), the heat capacity contour is constant and equals unity.

Figure 9 depicts the impact of the Stefan number and non-dimensional fusion temperature on the average Nusselt numbers of the fluid and solid matrix. Lower Stefan numbers specify higher latent heat of the PCM core and the heat capacity of the NEPCM, resulting in progressive augmentation in the rate of heat transfer. For each value of the Stefan number, the highest Nusselt numbers can be achieved when the fusion temperature is around 0.5. As discussed before, this is due to the fact for this case, the heat capacity increment leads to a higher temperature gradient and thus higher Nusselt numbers. This can be manifestly observed from the variation of the local Nusselt numbers of the fluid and solid presented in Figure 10. The vertical dash-dotted lines are used to separate the regions to ease the reading and comparison of the local Nusselt numbers of each graph. As seen, the location of these regions depends on the fusion temperature, indicating a local increment in the values of the heat transfer. As seen in Figure 9, the variation of Nu_s as a function of fusion temperature θ_f is not symmetric. When the fusion temperature is to low, the heat transfer at the hot wall is slightly higher than when the fusion temperature is about the temperature of the hot wall. The NEPCMs with a low fusion temperature creates a higher temperature gradient in the solid matrix next to the hot wall due to interaction between the liquid and the porous matrix, which leads to the improvement of the heat transfer rate compared to the case of NEPCMs with a high fusion temperature.

The variation of the total heat transfer ratio with the fusion temperature is shown in Figure 11. As discussed before, the highest heat transfer can be achieved for lower values of the Stefan numbers and at the fusion temperatures identical to the average temperature of the hot and cold walls (i.e., $\theta_f = 0.5$). In addition to this, for poor thermal conductivity of the porous medium like glass balls (LTE condition), adding 5% of the nano-encapsulated phase change materials to pure water can boost the rate of heat transfer up to 47% (for $Ste = 0.2$ and $\theta_f = 0.5$).

The dependency of the total heat transfer and total heat transfer ratio to the solid-fluid interface heat transfer parameter, volume fraction of NEPCM particles and the thermal conductivity of the solid matrix is depicted in Figure 12. As discussed before, increasing the thermal conductivity of the porous medium and the interface heat parameter boosts the total rate of heat transfer. In addition to this, for low values of the k_s, a direct correlation can be found between the overall rate of heat transfer and the volume fraction of the NEPCMs. Furthermore, for the case of glass balls ($k_s = 1.05$), increasing the interface parameter has a negligible impact on the rate of heat transfer. However, for a highly conductive solid matrix, the rate of heat transfer depends on whether LTNE or LTE is established. According to the results, although the overall rate of heat transfer is higher when the phases are in the state of thermal equilibrium ($H = 10^5$), the Q_r is lower when the LTE is validated between the phases.

To analyze the influence of the discussed parameters on the rate of heat transfer, more precisely, their impacts on the average Nusselt numbers of the solid and fluid phases are presented in Figure 13. As seen, by increasing the φ, and for all values of the k_s and H, the average Nusselt number of the fluid increases, and its solid counterpart decreases. This can be explained that increasing the volume fraction of the NEPCMs, as shown in Figure 8, slightly reduces the temperature gradients of the fluid and solid phases. On the other hand, increasing the φ intensifies the thermal conductivity of the suspension (Eqn 17). The figure for the fluid Nusselt number shows an upward trend indicating that the increment of the k_{nf} can compensate for the reduction of the fluid temperature gradient. However, for the solid phase, the solid Nusselt number decreases with the increment of the NEPCMs' volume fraction, and its reduction is more severe when the phases are in the state of thermal equilibrium ($H = 10^5$). As a result, the total heat transfer decreases when the reduction rate of heat transfer in the solid is more than its increase in the suspension.

5. Conclusion

Free convection of a suspension comprising nano-encapsulated phase change materials in a porous medium is analyzed. The capsules are made up of a core, which is the phase change material and a shell. The shell prevents the leakage and direct contact of the PCM to the host fluid. The thermophysical properties of the NEPCMs' core and shell are evaluated using a mixture model. As such, their latent heat during the phase change process is reflected in the heat capacity of the suspension, and thus, a temperature-dependent heat capacity can be found for the slurry. The sidewalls of the considered cavity are subjected to a temperature difference, and the other walls are well insulated. The local thermal non-equilibrium condition is considered between the fluid and the porous matrix. The non-linear governing equations, including the continuity and momentum equations for the nanofluid and energy equations for the phases, are first non-dimensionalized and then solved using the Galerkin finite element method. The influence of various involved parameters and non-dimensional numbers are surveyed on the patterns of the fluid and solid isotherms, streamlines, and the contours of the heat capacity ratio. The impact of these parameters on the local and average Nusselt numbers of the phases and the overall heat transfer ratio is studied as well. The following conclusions are achieved:

1. The non-dimensional fusion temperature can change the patterns of the fluid and solid isotherms and the streamlines. Indeed, the fusion temperature affects the heat capacity ratio around its corresponding fluid isotherm. The flow and thermal fields are more influenced when $\theta_f = 0.5$.
2. Increasing thermal conductivity of the porous medium boosts the rate of heat transfer and amplifies the fluid flow inside the cavity, and as a result, more capsules undergo the phase change.
3. Due to the augmentation of the viscosity, adding nano-encapsulated phase change materials to the base fluid reduces the fluid flow. In addition to this, the increasing volume fraction of the NEPCMs leads to a slight decrease in the temperature gradient of the fluid and solid.
4. The rate of transferred heat in the cavity is intensified with lower values of the Stefan numbers. In addition to this, the results show that regardless of the values of the Stefan number, the maximum rates of heat transfer for both fluid and solid can be achieved when the dimensionless fusion temperature is around 0.5. Furthermore, the graphs of local Nusselt numbers manifest that the influence of adding NEPCMs reflects in local augmentation of heat transfer, and the location of this augmentation is almost coincident with the corresponding isothermal line.
5. The heat transfer ratio, which is a measure of the amplification of the heat transfer rate with the presence of the NEPCMs, shows that adding 5% of the nano-encapsulated phase change materials to pure water can boost the rate of heat transfer up to 47% when the porous matrix is made up of glass balls (for $Ste = 0.2$ and $\theta_f = 0.5$).
6. For low values of the solid matrix's thermal conductivity, a direct correlation can be found between the overall rate of heat transfer and the volume fraction of the NEPCMs.
7. For porous mediums with high thermal conductivity, the influence of the heat transfer parameter is more pronounced. The rate of heat transfer intensifies when the phases are in the state of thermal equilibrium, but it decreases as the volume fraction of NEPCMs increases.
8. In contrast with the case of solid matrix with poor thermal conductivity, the total heat transfer ratio shows a downward trend with the NEPCMs' volume fraction when the LTE condition is established, and the thermal conductivity of porous medium is high, indicating that the incorporation of NEPCMs is more efficient when the thermal conductivity of solid matrix is poor. In other words, utilizing NEPCMs in a highly conductive solid matrix is more efficient only when the phases are in the state of local thermal non-equilibrium.

Declarations

Author contribution statement

Mohammad Ghalambaz & S.A.M. Mehryan: Conceived and designed the experiments; Wrote the paper.

Seyed Mohsen Hashem Zadeh: Performed the experiments; Analyzed and interpreted the data; Wrote the paper.

Amir Haghparast: Performed the experiments.

Hossein Zargartalebi: Analyzed and interpreted the data; Wrote the paper.

Competing interest statement

The authors declare no conflict of interest.

Additional information

No additional information is available for this paper.

References

[1] C. Kaviarasu, D. Prakash, Review on phase change materials with nanoparticle in engineering applications, J. Engin. Sci. Technol. Rev. 9 (4) (2016).

[2] A. Sharma, V.V. Tyagi, C. Chen, D. Buddhi, Review on thermal energy storage with phase change materials and applications, Renew. Sustain. Energy Rev. 13 (2) (2009) 318–345.

[3] Y. Tian, C.-Y. Zhao, Thermal analysis in phase change materials (PCMs) embedded with metal foams. 14th International Heat Transfer Conference, American Society of Mechanical Engineers Digital Collection, 2011, 2010, pp. 425–434.

[4] J.M. Mahdi, E.C. Nsofor, Melting enhancement in triplex-tube latent heat energy storage system using nanoparticles-metal foam combination, Appl. Energy 191 (2017) 22–34.

[5] F. Zhu, C. Zhang, X. Gong, Numerical analysis on the energy storage efficiency of phase change material embedded in finned metal foam with graded porosity, Appl. Therm. Eng. 123 (2017) 256–265.

[6] Y. Xu, M.-J. Li, Z.-J. Zheng, X.-D. Xue, Melting performance enhancement of phase change material by a limited amount of metal foam: configurational optimization and economic assessment, Appl. Energy 212 (2018) 868–880.

[7] X. Tong, J.A. Khan, E. RuhulAmin, Enhancement of heat transfer by inserting a metal matrix into a phase change material, Numer. Heat Tran. 30 (2) (1996) 125–141.

[8] H. Shokouhmand, B. Kamkari, Numerical simulation of phase change thermal storage in finned double-pipe heat exchanger. Applied Mechanics and Materials, Trans Tech Publ, 2012, pp. 742–746.

[9] L. Khatra, H. El Qarnia, The effect of the lower fin position on the PCM solidification process in a finned rectangular enclosure. 2015 3rd International Renewable and Sustainable Energy Conference (IRSEC), IEEE, 2015, pp. 1–6.

[10] Z. Qin, C. Ji, Z. Low, S. Dubey, F.H. Choo, F. Duan, Effect of fin location on the latent heat storage: a numerical study, Energy Procedia 143 (2017) 320–326.

[11] M.M. Joybari, F. Haghighat, S. Seddegh, A.A. Al-Abidi, Heat transfer enhancement of phase change materials by fins under simultaneous charging and discharging, Energy Convers. Manag. 152 (2017) 136–156.

[12] M. Jourabian, M. Farhadi, Melting of nanoparticles-enhanced phase change material (NEPCM) in vertical semicircle enclosure: numerical study, J. Mech. Sci. Technol. 29 (9) (2015) 3819–3830.

[13] M. Ghalambaz, A. Doostani, A.J. Chamkha, M.A. Ismael, Melting of nanoparticles-enhanced phase-change materials in an enclosure: effect of hybrid nanoparticles, Int. J. Mech. Sci. 134 (2017) 85–97.

[14] N.S. Bondareva, B. Buonomo, O. Manca, M.A. Sheremet, Heat transfer performance of the finned nano-enhanced phase change material system under the inclination influence, Int. J. Heat Mass Tran. 135 (2019) 1063–1072.

[15] R. Hossain, S. Mahmud, A. Dutta, I. Pop, Energy storage system based on nanoparticle-enhanced phase change material inside porous medium, Int. J. Therm. Sci. 91 (2015) 49–58.

[16] H.R. Seyf, Z. Zhou, H. Ma, Y. Zhang, Three dimensional numerical study of heat-transfer enhancement by nano-encapsulated phase change material slurry in microtube heat sinks with tangential impingement, Int. J. Heat Mass Tran. 56 (1-2) (2013) 561–573.

[17] S. Park, Y. Lee, Y.S. Kim, H.M. Lee, J.H. Kim, I.W. Cheong, W.-G. Koh, Magnetic nanoparticle-embedded PCM nanocapsules based on paraffin core and polyurea shell, Colloid. Surface. Physicochem. Eng. Aspect. 450 (2014) 46–51.

[18] C. Liu, Z. Rao, J. Zhao, Y. Huo, Y. Li, Review on nanoencapsulated phase change materials: preparation, characterization and heat transfer enhancement, Nano Energy 13 (2015) 814–826.

[19] K. Tumirah, M. Hussein, Z. Zulkarnain, R. Rafeadah, Nano-encapsulated organic phase change material based on copolymer nanocomposites for thermal energy storage, Energy 66 (2014) 881–890.

[20] S. Wu, H. Wang, S. Xiao, D. Zhu, An investigation of melting/freezing characteristics of nanoparticle-enhanced phase change materials, J. Therm. Anal. Calorim. 110 (3) (2012) 1127–1131.

[21] S. Motahar, N. Nikkam, A.A. Alemrajabi, R. Khodabandeh, M.S. Toprak, M. Muhammed, A novel phase change material containing mesoporous silica nanoparticles for thermal storage: a study on thermal conductivity and viscosity, Int. Commun. Heat Mass Tran. 56 (2014) 114–120.

[22] M. Ghalambaz, S.M. Hashem Zadeh, S.A.M. Mehryan, K. Ayoubi Ayoubloo, N. Sedaghatizadeh, Non-Newtonian behavior of an electrical and magnetizable phase change material in a filled enclosure in the presence of a non-uniform magnetic field, Int. Commun. Heat Mass Tran. 110 (2020) 104437.

[23] M.S. Al-Jethelah, S.H. Tasnim, S. Mahmud, A. Dutta, Melting of nano-phase change material inside a porous enclosure, Int. J. Heat Mass Tran. 102 (2016) 773–787.

[24] S. Sahoo, M. Das, P. Rath, Numerical study of cyclic melting and solidification of nano enhanced phase change material based heat sink in thermal management of electronic components, ASME 2016 5th International Conference on Micro/Nanoscale Heat and Mass Transfer, American Society of Mechanical Engineers Digital Collection, 2016.

[25] W. Alshaer, S. Nada, M. Rady, C. Le Bot, E.P. Del Barrio, Numerical investigations of using carbon foam/PCM/Nano carbon tubes composites in thermal management of electronic equipment, Energy Convers. Manag. 89 (2015) 873–884.

[26] N.H. Boukani, A. Dadvand, A. Chamkha, Melting of a Nano-enhanced Phase Change Material (NePCM) in partially-filled horizontal elliptical capsules with different aspect ratios, Int. J. Mech. Sci. 149 (2018) 164–177.

[27] M. Abdollahzadeh, M. Esmaeilpour, Enhancement of phase change material (PCM) based latent heat storage system with nano fluid and wavy surface, Int. J. Heat Mass Tran. 80 (2015) 376–385.

[28] M. Jourabian, M. Farhadi, K. Sedighi, On the expedited melting of phase change material (PCM) through dispersion of nanoparticles in the thermal storage unit, Comput. Math. Appl. 67 (7) (2014) 1358–1372.

[29] R. Sharma, P. Ganesan, J. Sahu, H. Metselaar, T. Mahlia, Numerical study for enhancement of solidification of phase change materials using trapezoidal cavity, Powder Technol. 268 (2014) 38–47.

[30] S. Hoseinzadeh, R. Ghasemiasl, D. Havaei, A.J. Chamkha, Numerical investigation of rectangular thermal energy storage units with multiple phase change materials, J. Mol. Liq. 271 (2018) 655–660.

[31] S. Barlak, O.N. Sara, A. Karaipekli, S. Yapıcı, Thermal conductivity and viscosity of nanofluids having nanoencapsulated phase change material, Nanoscale Microscale Thermophys. Eng. 20 (2) (2016) 85–96.

[32] M. Ghalambaz, A.J. Chamkha, D. Wen, Natural convective flow and heat transfer of Nano-Encapsulated Phase Change Materials (NEPCMs) in a cavity, Int. J. Heat Mass Tran. 138 (2019) 738–749.

[33] A. Hajjar, S. Mehryan, M. Ghalambaz, Time periodic natural convection heat transfer in a nano-encapsulated phase-change suspension, Int. J. Mech. Sci. (2019) 105243.

[34] D.B. Ingham, I. Pop, Transport Phenomena in Porous media III, Elsevier, 2005.

[35] H. Zargartalebi, A. Noghrehabadi, M. Ghalambaz, I. Pop, Natural convection boundary layer flow over a horizontal plate embedded in a porous medium saturated with a nanofluid: case of variable thermophysical properties, Transport Porous Media 107 (1) (2015) 153–170.

[36] M. Ghalambaz, H. Hendizadeh, H. Zargartalebi, I. Pop, Free convection in a square cavity filled with a tridisperse porous medium, Transport Porous Media 116 (1) (2017) 379–392.

[37] H. Zargartalebi, M. Ghalambaz, K. Khanafer, I. Pop, Unsteady conjugate natural convection in a porous cavity boarded by two vertical finite thickness walls, Int. Commun. Heat Mass Tran. 81 (2017) 218–228.

[38] A.I. Alsabery, R. Mohebbi, A.J. Chamkha, I. Hashim, Effect of local thermal non-equilibrium model on natural convection in a nanofluid-filled wavy-walled porous cavity containing inner solid cylinder, Chem. Eng. Sci. 201 (2019) 247–263.

[39] A.J. Chamkha, S. Sazegar, E. Jamesahar, M. Ghalambaz, Thermal non-equilibrium heat transfer modeling of hybrid nanofluids in a structure composed of the layers of solid and porous media and free nanofluids, Energies 12 (3) (2019) 541.

[40] M.A. Sheremet, I. Pop, Effect of local heater size and position on natural convection in a tilted nanofluid porous cavity using LTNE and Buongiorno's models, J. Mol. Liq. 266 (2018) 19–28.

[41] H. Zargartalebi, M. Ghalambaz, A. Noghrehabadi, A.J. Chamkha, Natural convection of a nanofluid in an enclosure with an inclined local thermal non-equilibrium porous fin considering Buongiorno's model, Numer. Heat Tran. Part A: Appl. 70 (4) (2016) 432–445.

[42] M. Izadi, G. Hoghoughi, R. Mohebbi, M. Sheremet, Nanoparticle migration and natural convection heat transfer of Cu-water nanofluid inside a porous undulant-wall enclosure using LTNE and two-phase model, J. Mol. Liq. 261 (2018) 357–372.

[43] S. Sivasankaran, A. Alsabery, I. Hashim, Internal heat generation effect on transient natural convection in a nanofluid-saturated local thermal non-equilibrium porous inclined cavity, Phys. Stat. Mech. Appl. 509 (2018) 275–293.

[44] S. Mehryan, M.A. Sheremet, M. Soltani, M. Izadi, Natural convection of magnetic hybrid nanofluid inside a double-porous medium using two-equation energy model, J. Mol. Liq. 277 (2019) 959–970.

[45] M. Ghalambaz, T. Groşan, I. Pop, Mixed convection boundary layer flow and heat transfer over a vertical plate embedded in a porous medium filled with a suspension of nano-encapsulated phase change materials, J. Mol. Liq. 293 (2019) 111432.

[46] M. Ghalambaz, S. Mehryan, A. Hajjar, A. Veisimoradi, Unsteady Natural Convection Flow of a Suspension Comprising Nano-Encapsulated Phase Change Materials (NEPCMs) in a Porous Medium, Advanced Powder Technology, 2019.

[47] D.A. Nield, A. Bejan, Convection in Porous Media, Springer, 2017.

[48] L. Chai, R. Shaukat, L. Wang, H.S. Wang, A review on heat transfer and hydrodynamic characteristics of nano/microencapsulated phase change slurry (N/MPCS) in mini/microchannel heat sinks, Appl. Therm. Eng. 135 (2018) 334–349.

[49] B. Chen, X. Wang, R. Zeng, Y. Zhang, X. Wang, J. Niu, Y. Li, H. Di, An experimental study of convective heat transfer with microencapsulated phase change material suspension: laminar flow in a circular tube under constant heat flux, Exp. Therm. Fluid Sci. 32 (8) (2008) 1638–1646.

[50] K. Khanafer, K. Vafai, A critical synthesis of thermophysical characteristics of nanofluids, Int. J. Heat Mass Tran. 54 (19-20) (2011) 4410–4428.

[51] A. Zaraki, M. Ghalambaz, A.J. Chamkha, M. Ghalambaz, D. De Rossi, Theoretical analysis of natural convection boundary layer heat and mass transfer of nanofluids: effects of size, shape and type of nanoparticles, type of base fluid and working temperature, Adv. Powder Technol. 26 (3) (2015) 935–946.

[52] A. Chamkha, A. Doostanidezfuli, E. Izadpanahi, M. Ghalambaz, Phase-change heat transfer of single/hybrid nanoparticles-enhanced phase-change materials over a heated horizontal cylinder confined in a square cavity, Adv. Powder Technol. 28 (2) (2017) 385–397.

[53] J. Buongiorno, D.C. Venerus, N. Prabhat, T. McKrell, J. Townsend, R. Christianson, Y.V. Tolmachev, P. Keblinski, L.-w. Hu, J.L. Alvarado, A benchmark study on the thermal conductivity of nanofluids, J. Appl. Phys. 106 (9) (2009), 094312.

[54] D.C. Venerus, J. Buongiorno, R. Christianson, J. Townsend, I.C. Bang, G. Chen, S.J. Chung, M. Chyu, H. Chen, Y. Ding, Viscosity measurements on colloidal dispersions (nanofluids) for heat transfer applications, Appl. Rheol. 20 (4) (2010) 11–17.

[55] M. Ghalambaz, A. Doostani, E. Izadpanahi, A. Chamkha, Phase-change heat transfer in a cavity heated from below: the effect of utilizing single or hybrid nanoparticles as additives, J. Taiwan Inst. Chem. Eng. 72 (2017) 104–115.

[56] O. Schenk, K. Gärtner, Solving unsymmetric sparse systems of linear equations with PARDISO, Future Generat. Comput. Syst. 20 (3) (2004) 475–487.

[57] P. Wriggers, Nonlinear Finite Element Methods, Springer Science & Business Media, 2008.

[58] F. Verbosio, A. De Coninck, D. Kourounis, O. Schenk, Enhancing the scalability of selected inversion factorization algorithms in genomic prediction, J. Comput. Sci. 22 (2017) 99–108.

[59] O.C. Zienkiewicz, R.L. Taylor, The Finite Element Method for Solid and Structural Mechanics, Elsevier, 2005.

[60] K. Kahveci, Buoyancy driven heat transfer of nanofluids in a tilted enclosure, J. Heat Tran. 132 (6) (2010), 062501.

[61] A.C. Baytas, I. Pop, Free convection in a square porous cavity using a thermal nonequilibrium model, Int. J. Therm. Sci. 41 (9) (2002) 861–870.